Conductivity, Electrodeposition and Magnetic Property of Cobalt(II) and Dysprosium Chloride in Zinc Chloride-1-Ethyl-3-Methylimidazolium Chloride Room Temperature Molten Salt

Hsin-Yi Hsu and Chao-Chen Yang

Graduate School of Engineering Science & Technology (Doctoral Program), National Yunlin University of Science and Technology, 123 University Road, Sec. 3, Touliu, Yunlin, Taiwan 640, R. O. C.

Reprint requests to Prof. C.-C. Yang. Fax: 886-5-531-2056; E-mail: yangcc@flame.yuntech.edu.tw

Z. Naturforsch. **58b,** 139 – 146 (2003); received August 20, 2002

Electric conductivity of the molten zinc chloride-1-ethyl-3-methylimidazolium chloride phases has been measured by a computerized system using the d.c. four-probes method. The sequence of the conductivities for the different component melts is $ZnCl_2$-EMIC > $ZnCl_2$-EMIC-$CoCl_2$ > $ZnCl_2$-EMIC-$DyCl_3$ > $ZnCl_2$-EMIC-$CoCl_2$-$DyCl_3$. The results may be explained in terms of the viscosity increase due to the complex formation.

The electrochemistry and the nucleation mechanism of cobalt(II) or/and dysprosium chloride in acidic $ZnCl_2$-EMIC melts have been investigated by cyclic voltammetry and chronoamperometry at different temperatures, respectively. The results of the SEM and VSM analyses reveal that reduction of Dy^{3+} to Dy^{2+} may have occurred, while reduction of Dy^{3+} to Dy(0) is conjectured to play no role. Moreover, the results of chronoamperometry experiments show that nucleation in the alloy electrodeposition is instantaneous, and that, as the applied deposition potential becomes more negative, the nucleation density increases, which rapidly shortens the time required for the diffusion zones to overlap.

Electrodeposition of a Dy-Co-Zn alloy on a Ni or Cu sheet from the 50-50 mol% $ZnCl_2$-EMIC melt containing 1.687 mol% $CoCl_2$ and 1.114 mol% $DyCl_3$ has been accomplished, and the morphology and the composition have been analyzed by SEM and EDS, respectively. The magnetism of the deposited layer is discussed based on the results of the VSM analysis.

Key words: Conductivity, Cyclic Voltammetry, Electrodeposition, Magnetic Property

Introduction

In recent years, transition metal (TM) and rare-earth (RE) elements and their compounds have drawn considerable attention as materials for electric, magnetic, optical, and anti-corrosion purposes, superconductors and catalytic reactions. Thin films based on RE and TM elements have been attractive materials for magneto-optical (MO) data storage. According to research reports, Beach *et al.* [1] report that the Curie temperature of dysprosium can be increased by several tens of degrees when dysprosium is grown on lutetium. Sagawa *et al.* [2] find that addition of Dy increases the anisotropy coefficient of the $Nd_2Fe_{14}B$ phase commonly made to commercial magnets to give increased coercitivity. Mohan and Kronmüller [3] report that very high coercive fields have been observed at low temperature in an amorphous $(Tb_{0.27}Dy_{0.73})_{0.32}Fe_{0.68}$ sputter deposited thin film. Papakonstantinou *et al.* [4] explored the effects of substrate temperature and oxygen pressure on pulsed laser deposited Bi-substituted Dy iron garnet films, and the results indicate that the coercivity could reach several kOe. The magnetism of amorphous SmDyFeCo films deposited by RF-magnetron sputtering were studied by Lu *et al.* [5], and the results exhibit that when Sm is substituted for Dy, the compensation temperature T_{comp} decreases, the Curie temperature T_c remains unchanged, the Kerr rotation angle θ_k increases, the saturation magnetization M_s at the room temperature increases, and changes slowly with the temperature, and the coercivity H_c remains high in a wide range of the temperature. Consequently, the effects of RE elements in MO thin films are of considerable interest.

Owing to the demand for optical data storage, reading and writing, preparation of MO thin films has been a major challenge all over the world. However, sputtering and molecular beam epitaxy (MBE) as employed

for the preparation of MO thin films need expensive equipment [6 – 8], and, further, are not feasible to obtain thin films on large area substrates. Hence, a better and more economic method for the preparation is desirable. Electrodeposition may be implemented with a basically simple equipment. Not to mention, it is very simple to prepare deposit film of desired thickness by controlling the electroplating time or the current density. Nevertheless, the fabrication of the MO thin film with electrodeposition from room-temperature molten salts (RTMS) has not been investigated.

Molten salts are aprotic solvents and possess some unique properties, *e. g.*, high conductivity, a wide electrochemical window and low vapor pressure. It can be used to overcome hydrogen embrittlement and low current efficiency. Moreover, the melting points of RTMS are low and therefore the handling is easier. Sun *et al.* [9] have studied electrodepositions of Co and Co—Zn alloys from the acidic $ZnCl_2$-EMIC RTMS. However, the conductivities of such mixed melts have not been reported and the electrochemistry and electrodeposition of Dy—Co—Zn alloys from acidic $ZnCl_2$-EMIC melts have not been investigated, either.

In the present study, electric conductivities of $ZnCl_2$-EMIC, $ZnCl_2$-EMIC-$CoCl_2$, $ZnCl_2$-EMIC-$DyCl_3$ and $ZnCl_2$-EMIC-$CoCl_2$-$DyCl_3$ melts have been measured, and the electrochemistry and nucleation mechanism of cobalt(II) and dysprosium chlorides in acidic 50-50 mol% $ZnCl_2$-EMIC melts investigated by cyclovoltammetry and chronoamperometry, respectively. The electrodeposition of the alloys has been performed on Ni and Cu substrates by controlled potential coulometry, and the morphology, composition and magnetic properties of the electrodeposited layers have been analyzed by SEM (scanning electron microscopy), EDS (energy dispersive X-ray spectroscopy) and VSM (vibrating sample magnetometry), respectively.

Experimental Section

$ZnCl_2$ (Merck, anhydrous, 98%), EMIC (1-ethyl-3-methylimidazolium chloride, Aldrich, 98%), $CoCl_2$ (Merck, anhydrous, 99%) and $DyCl_3$ (Acros, anhydrous, 99.9%) were used as received. The molten salts with different compositions were prepared by continuous stirring for 12 h and left for 12 h without further stirring under a purified nitrogen atmosphere in a glove box. The electrical conductivities of these melts were measured by a computerized system using the d.c. four-probes method described in [10].

The electrochemical experiments were performed in a sealed three-electrode electrochemical cell. The nickel (0.031 cm^2) or copper (0.1571 cm^2) working electrode was made by winding a Teflon tape around a nickel rod (Gredmann, 99.2%) or a copper rod (Nilaco, 99.99%) and inserting it into a glass tube. The electrode was polished successively with increasingly finer grades of emery paper, finally followed by rinsing with distilled water and dried under a vacuum. The counter electrode was a zinc spiral (Nilaco, 99.9%) connected to a Pt wire sealed in a glass tube and immersed in the bulk electrolyte melt. The reference electrode was also a zinc wire immersed in a pure 50-50 mol% $ZnCl_2$-EMIC melt contained in a sealed Pt wire glass tube. The electrochemical behavior and the nucleation mechanism of melts were studied on the Ni and Cu substrates by cyclic voltammetry and chronoamperometry, respectively, with an EG&G model 273A potentiostat/galvanostat controlled with an EG&G model 270/250 software. The electrodeposition of alloys was also performed at different potentials by controlled potential coulometry. At the end of the experiment, the electrodes were taken out from the molten electrolytes, washed with dry propylene carbonate, ethanol, and deionized water and, after slight supersonic rinsing, dried and stored in a desiccator for further analysis. The morphology and composition of the electrodeposited layer were determined by SEM (scanning electron microscopy) and EDS (energy dispersive X-ray spectroscopy), respectively, and the magnetic properties were examined by the VSM (vibrating sample magnetometry).

Results and Discussion

The conductivities of the 50-50 mol% $ZnCl_2$-EMIC melts containing different components are shown as a function of temperature in Fig. 1. The experimental data were least-squares fitted to equations of the form $\sigma = a + bT + cT^2$, where T is the temperature in °C. The obtained parameters a, b and c are given in Table 1. As the squared R values are larger than 0.998, the above equations fit the experimental data very well. Fig. 1 shows that the conductivities of all melts increase nearly linearly with temperature, and that the sequence of the conductivities for the different component melts is $ZnCl_2$-EMIC $>$ $ZnCl_2$-EMIC-$CoCl_2$ $>$ $ZnCl_2$-EMIC-$DyCl_3$ $>$ $ZnCl_2$-EMIC-$CoCl_2$-$DyCl_3$. The results may be explained in terms of the viscosity increase due to complex formation. Close observation reveals that the sequence of viscosity for these melts is $ZnCl_2$-EMIC-$CoCl_2$-$DyCl_3$ $>$ $ZnCl_2$-EMIC-$DyCl_3$ $>$ $ZnCl_2$-EMIC-$CoCl_2$ $>$ $ZnCl_2$-EMIC. The viscosity increase of the melts containing $CoCl_2$ or/and $DyCl_3$

Melt component	$a/10^{-2}\,S\cdot cm^{-1}$	$b/10^{-4}\,S\cdot cm^{-1}$	$c/10^{-6}\,S\cdot cm^{-1}$	R squared	t / °C
blank	−0.996	1.4594	1.8778	0.9994	70-150
1.687 mol% $CoCl_2$	−1.5099	2.615	1.0826	0.9982	70-150
1.114 mol% $DyCl_3$	−1.1098	1.5703	1.4956	0.9990	70-150
1.687 mol% $CoCl_2$ +1.114 mol% $DyCl_3$	−0.35	−0.00425	2.0567	0.9997	70-150

Table 1. Parameters for the electrical conductivity equation of 50-50 mol% $ZnCl_2$-EMIC with different components: $\sigma = a + bt + ct^2$.

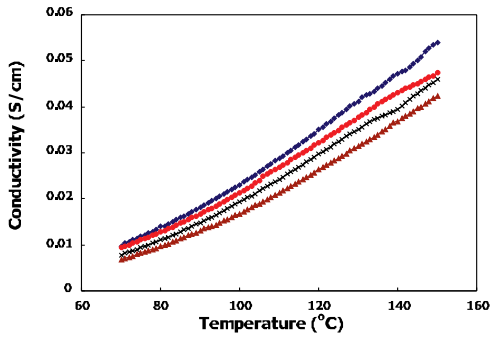

Fig. 1. The conductivities of the 50-50 mol% $ZnCl_2$-EMIC melts containing different components as a function of temperature. Components: ◆: blank; ●: 1.687 mol% $CoCl_2$; ✕: 1.114 mol% $DyCl_3$; ▲: 1.687 mol% $CoCl_2$ and 1.114 mol% $DyCl_3$.

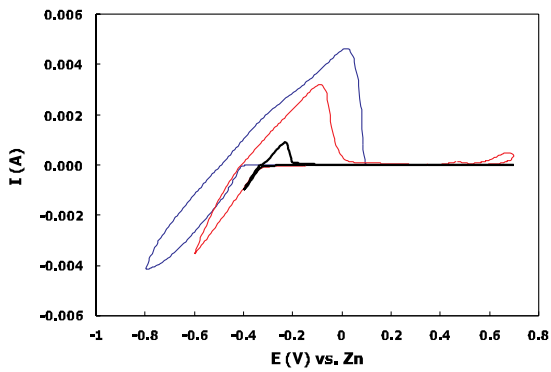

Fig. 2. Cyclic voltammograms for the 50-50 mol% $ZnCl_2$-EMIC melt on the Ni electrode at 80 °C under different scan reverses. Scan rate: 50 mV/s.

seems to parallel the decrease in conductivity. Furthermore, since the formation of complex ions by a transition metal (Co) and a rare-earth element (Dy) is expected to occur very readily, reduced mobility of ions in the melts is instantaneous and the conductivity of the melts containing $CoCl_2$ or / and $DyCl_3$ decreases.

The electrochemical behavior of cobalt(II) and dysprosium chlorides in 50-50 mol% $ZnCl_2$-EMIC melts at various temperatures has been investigated by cyclic voltammetry. The cyclic voltammograms (Ni working

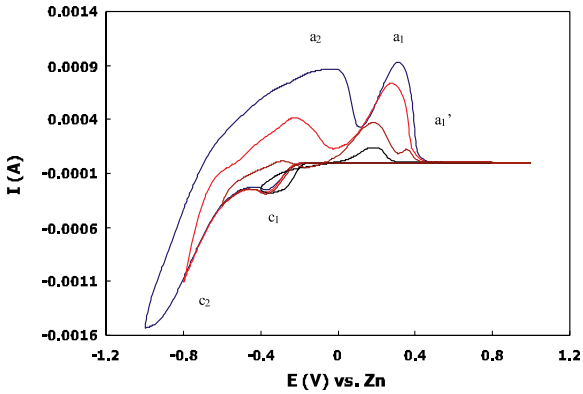

Fig. 3. Cyclic voltammograms for the 50-50 mol% $ZnCl_2$-EMIC melt with 1.687 mol% $CoCl_2$ on the Ni electrode at 100 °C under different scan reverses. Scan rate: 50 mV/s.

electrode at 80 °C) under different scan reverses are shown in Fig. 2 and exhibit a single reduction wave and an associated oxidation wave in the potential peak range between −0.22 and 0.02 V. The reduction wave must be due to the cathodic reduction of Zn(II) species to Zn metal. The oxidation wave must be due to the anodic stripping of the Zn metal which was deposited on the Ni electrode. When the scan reverse potential was shifted to a more negative potential (from −0.4 to −0.8 V), the oxidation potential also shifted to more positive values and the peak current increased. Zn metal deposited adequately on the Ni electrode at a −0.8 V scan reverse potential, which resulted in more positive oxidation potentials and larger peak currents than in the case of the scan reverse at −0.4 or −0.6 V.

Fig. 3 shows the cyclic voltammograms for the 50-50 mol% $ZnCl_2$-EMIC melt containing 1.687 mol% $CoCl_2$ on the Ni working electrode at 100 °C under different scan reverses. There are two reduction waves (c_1, c_2) and two major oxidation waves (a_1, a_2). The former must be due to the cathodic reduction of Co(II) (wave c_1) and Zn^{2+} species (wave c_2). Fig. 3 also exhibits the stripping wave (a_2) of the zinc deposit. The wave in the voltammograms of melts containing Co(II) is different from the one in the pure 50-50 mol% $ZnCl_2$-EMIC melt and appears in a broader

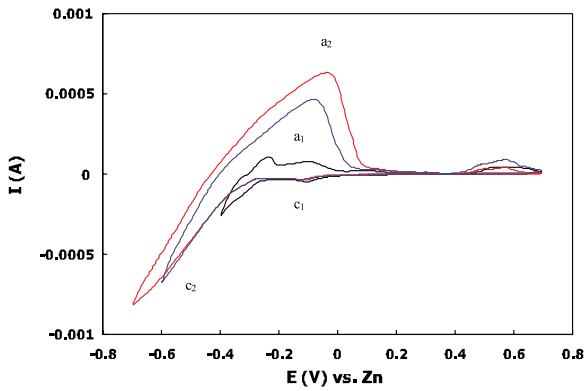

Fig. 4. Cyclic voltammograms for the 50-50 mol% $ZnCl_2$-EMIC melt with 1.114 mol% $DyCl_3$ on the Ni electrode at 100 °C under different scan reverses. Scan rate: 50 mV/s.

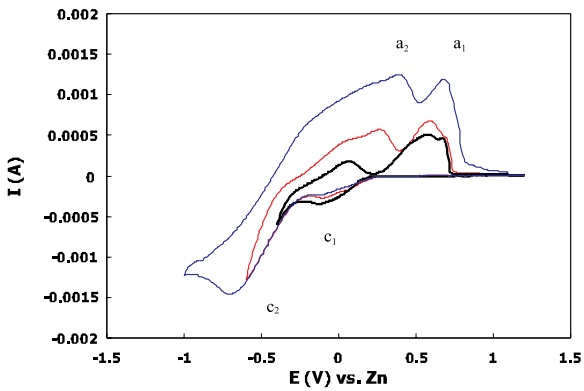

Fig. 5. Cyclic voltammograms for the 50-50 mol% $ZnCl_2$-EMIC melt with 1.687 mol% $CoCl_2$ and 1.114 mol% $DyCl_3$ on the Ni electrode at 100 °C under different scan reverses. Scan rate: 50 mV/s.

shape. Based on this observation, it is assumed that a Co—Zn alloy is electrodeposited and that the wave a_2 can be attributed to the oxidation of the Co—Zn alloy deposit. Moreover, the oxidation wave a_1 must be due to the anodic stripping of the cobalt that was electrodeposited on the Ni electrode at wave c_1; a small oxidation wave a_1' is also found in the voltammogram of Fig. 3 at the −0.6 V scan reverse potential, which is assumed to be due to oxidation of the cobalt interacting with the Ni substrate, because it is oxidized less readily than the bulk cobalt deposit.

Fig. 4 shows the cyclic voltammograms for the 50-50 mol% $ZnCl_2$-EMIC melt containing 1.114 mol% $DyCl_3$ on the Ni electrode at 100 °C with different scan reverses. There are two reduction waves (c_1, c_2) and a major oxidation wave (a_2), of which c_2 must be due to the reduction of Zn^{2+} species and a_2 to the associated oxidation wave, while c_1 is assigned to the reduction of Dy(III) to Dy(II) [11] or of Dy(III) to Dy, with a_1 being the associated oxidation wave.

The mixing enthalpies of liquid Dy—Co alloys have been reported [12]. The experiments were carried out using a twin solution calorimeter at 1818 K under purified He atmosphere. The data show that the formation of Dy—Co alloys is feasible at high temperature. Rare earth (RE) elements and cobalt form a unique group of intermetallic compounds possessing the hexagonal $CaCu_5$ structure. $RECo_5$ intermetallic compounds have received considerable attention, mainly due to the large magneto-crystalline anisotropy energy of $SmCo_5$ at low temperatures [13]. However, the electrochemistry and electrodeposition of Dy—Co or Dy—Co—Zn alloys from the RTMS have not been reported.

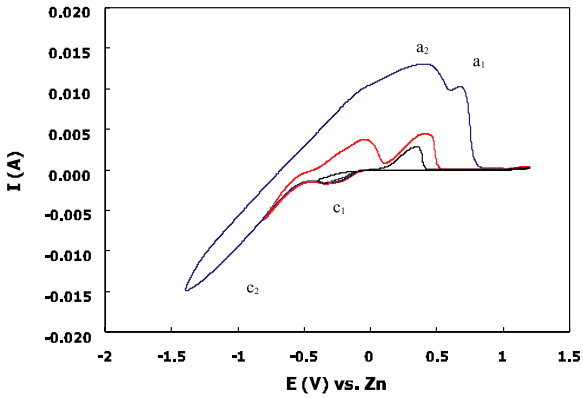

Fig. 6. Cyclic voltammograms for the 50-50 mol% $ZnCl_2$-EMIC melt with 1.687 mol% $CoCl_2$ and 1.114 mol% $DyCl_3$ on the Cu electrode at 80 °C under different scan reverses. Scan rate: 50 mV/s.

In order to investigate the feasibility of the preparation of Dy—Co or Dy—Co—Zn alloys from the RTMS, cyclic voltammetry for the 50-50 mol% $ZnCl_2$-EMIC melt containing 1.687 mol% $CoCl_2$ and 1.114 mol% $DyCl_3$ on a Ni and a Cu electrode at different temperatures under different scan reverses has been carried out, and the results are shown in Fig. 5 and Fig. 6, respectively. There are two reduction waves and two oxidation waves in Fig. 5. Wave c_2 must be due to the cathodic reduction of Zn^{2+} species, wave a_2 to the oxidation of the Co—Zn alloy deposit of Fig. 3; c_1 may be due to the cathodic reduction of Co^{2+} or Co^{2+}/Dy^{3+} species; a component analysis of the deposit is needed to confirm the reduction. Fig. 6 is similar to Fig. 5 with the waves c_1, c_2 shifted to more negative potential

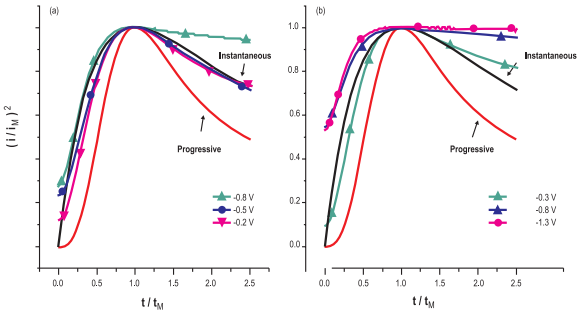

Fig. 7. Reduced-variable plots of current-time transients obtained with the 50-50 mol% $ZnCl_2$-EMIC melt with 1.687 mol% $CoCl_2$ and 1.114 mol% $DyCl_3$ on (a) the Ni electrode at 100 °C; (b) the Cu electrode at 80 °C. Theoretical curves for instantaneous and progressive nucleation are also shown for comparison.

(−0.2, −0.5, and −0.8 V on the Ni substrate and −0.3, −0.8, and −1.3 V on the Cu substrate).

In order to investigate the alloy nucleation/growth process, chronoamperometric studies were carried out on the Ni and Cu electrodes. Reduced-variable plots shown in Fig. 7 have been derived from the current-time transients to enable us to compare the results with the standard model for three-dimensional instantaneous and progressive nucleations [14]. The dimensionless experimental current-time transients resulted from chronoamperometry for the deposition of an alloy from the 50-50 mol% $ZnCl_2$-EMIC melt containing 1.687 mol% $CoCl_2$ and 1.114 mol% $DyCl_3$ on the Ni and Cu electrode.

Figure 7(a) shows that the nucleation is instantaneous for the alloy electrodeposition on the Ni electrode; however, as the applied deposition potential becomes more negative (−0.8 V), the nucleation density increases and this rapidly shortens the time required for the diffusion zones to overlap.

Figure 7(b) shows similar phenomena for the alloy electrodeposition on the Cu electrode; however, the diffusion zones rapidly overlap when the applied deposition potential becomes more negative (−0.8 and −1.3 V). That is to say, the diffusion current will more rapidly reach the Cottrell current [15] when the applied deposition potential is shifted to more negative values. It is conjectured that two dimensional nucleation on the Cu substrate surface is the most common nucleation process at high overpotentials.

The Dy—Co—Zn alloys were electrodeposited with a constant deposition potential on a Ni sheet at 100 °C and on a Cu sheet at 80 °C from 50-50 mol% $ZnCl_2$-EMIC melts containing 1.687 mol% $CoCl_2$ and 1.114 mol% $DyCl_3$. For all of the deposition experi-

Table 2. The composition of electrodeposited layers shown in Figs. 8 and 9 analyzed by EDS.

Substrate	Deposition potential (V)	Composition (wt%) Co	Zn	Dy
Ni	−0.2	84.38	1.97	13.65
	−0.5	46.84	28.63	24.54
	−0.8	34.29	43.04	22.67
Cu	−0.3	75.08	10.14	14.78
	−0.5	44.22	49.16	6.62
	−0.8	22.32	72.37	5.31
	−1.3	7.91	84.17	7.91

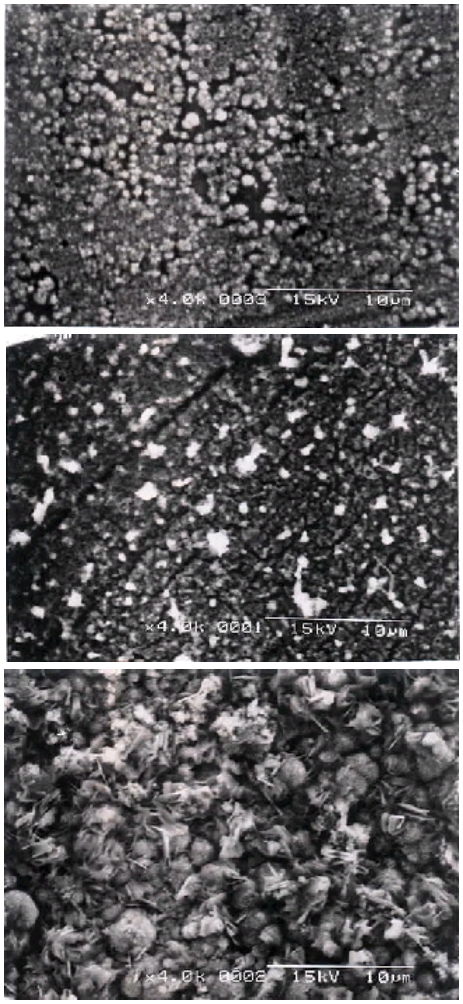

Fig. 8. SEM micrographs of Dy-Co-Zn layers electrodeposited from the 50-50 mol% $ZnCl_2$-EMIC melt with 1.687 mol% $CoCl_2$ and 1.114 mol% $DyCl_3$ on the Ni sheet at 100 °C. The electrodeposition potentials were (a) −0.2 V; (b) −0.5 V; (c) −0.8 V.

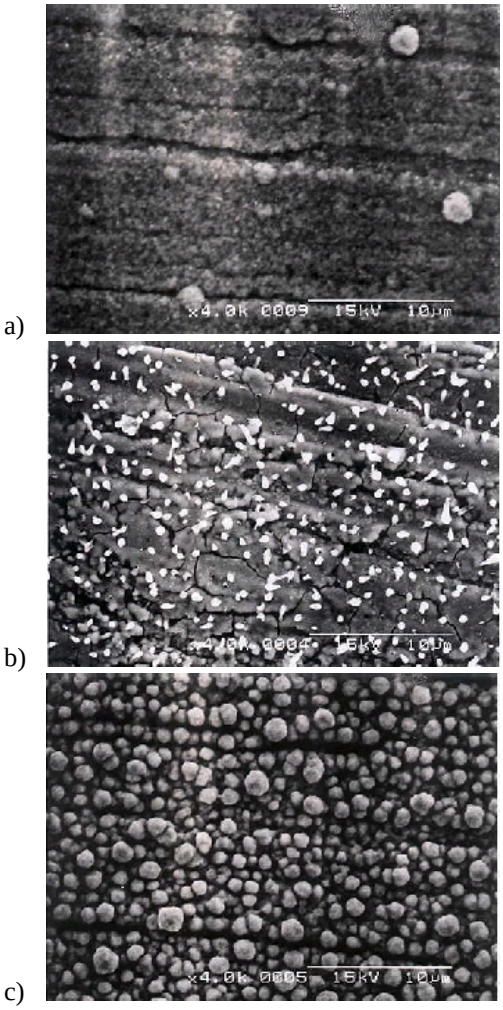

Fig. 9. SEM micrographs of Dy-Co-Zn layers electrodeposited from the 50-50 mol% $ZnCl_2$-EMIC melt with 1.687 mol% $CoCl_2$ and 1.114 mol% $DyCl_3$ on the Cu sheet at 80 °C. The electrodeposition potentials were (a) −0.3 V; (b) −0.8 V; (c) −1.3 V.

ments, a fixed amount of electricity was passed to make the comparison easier. The composition of the electrodeposits determined by EDS is given in Table 2. The data indicate that a less negative potential is more advantageous to the electrodeposition of the Co component, as also shown by the cyclic voltammograms in Figs 5 and 6. On the contrary, the Zn content of the deposited layer shows an opposite trend.

The Dy content in the deposited layer has been examined by EDS; in which form the component exists (Dy^{2+}, Dy^{3+} or Dy) has been explored by SEM and

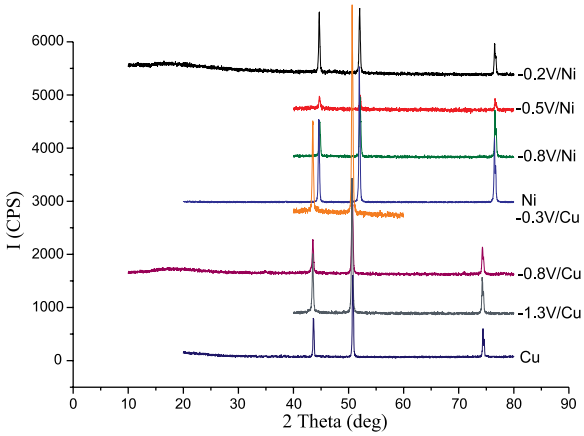

Fig. 10. XRD patterns of Dy-Co-Zn layers electrodeposited from the 50-50 mol% $ZnCl_2$-EMIC melt with 1.687 mol% $CoCl_2$ and 1.114 mol% $DyCl_3$ on the Ni and Cu sheet under different deposition potentials.

VSM analyses. The SEM micrographs are presented in Figs 8 and 9, respectively.

Fig. 8(a) exhibits the surface morphology of the fine grains deposited with the less negative deposition potential (−0.2 V), and Fig. 8(b) proves that, when a more negative potential (−0.5 V) is applied, a finer and denser deposited layer has been formed on the surface of which some particles are randomly dispersed. These particles are presumed to be $DyCl_3$ or $DyCl_2$ enclosed in the deposited layer by electromigration. An EDS analysis reveals that Dy is present. When the more negative deposition potential to −0.8 V is applied, Zn is the major component and its bigger grains and dendrites are present on the deposited layer. It is obvious that, as a less negative deposition potential is applied, finer grains and a layer with higher Co content can be deposited. The electrodeposited particle size of Co is smaller than that of Zn.

Figures 9(a) and (b) exhibit that the morphologies of the deposited layers on the Cu sheet are similar to those shown in Figs. 8(a) and (b), respectively. The layer on the Cu sheet is assumed to have better adhesion than that on the Ni sheet. Figure 9(c) shows that at −1.3 V particles of about 1 μm diameter have deposited on the Cu sheet. The layer electrodeposited at −1.3 V has a smooth crystalline surface, where the Zn content is 84.17 wt% from the EDS analysis. Electrodeposition of zinc is the major electrochemical reaction at more negative deposition potentials.

X-ray diffraction patterns of the deposited layers are shown in Fig. 10. It is observed that the XRD patterns

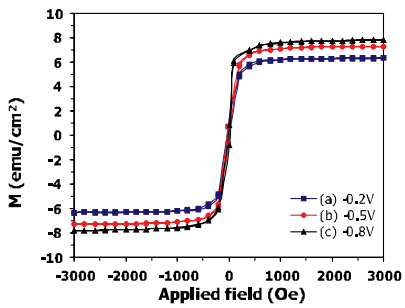

Fig. 11. Hysteresis loops of Dy-Co-Zn layers electrodeposited from the 50-50 mol% $ZnCl_2$-EMIC melt with 1.687 mol% $CoCl_2$ and 1.114 mol% $DyCl_3$ on the Ni sheet at 100 °C under different electrodeposition potentials. The coercive field H_c are (a) 28.3 Oe; (b) 23.7 Oe; (c) 23.9 Oe.

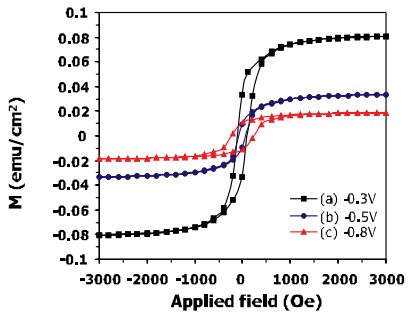

Fig. 12. Hysteresis loops of Dy-Co-Zn layers electrodeposited from the 50-50 mol% $ZnCl_2$-EMIC melt with 1.687 mol% $CoCl_2$ and 1.114 mol% $DyCl_3$ on the Cu sheet at 80 °C under different electrodeposition potentials. The coercive field H_c are (a) 102.6 Oe; (b) 69.2 Oe; (c) 236.5 Oe.

of these layers deposited on the Ni and Cu electrodes are similar to the pattern of the pure Ni and Cu, respectively. However, there is no other peak exhibited in Fig. 10, indicating that the structure of these deposited layers can be considered as the amorphous form.

Fig. 11 shows the hysteresis loops of Dy-Co-Zn layers electrodeposited from the 50-50 mol% $ZnCl_2$-EMIC melt containing 1.687 mol% $CoCl_2$ and 1.114 mol% $DyCl_3$ on the Ni sheet at 100 °C under different deposition potentials. The coercive fields H_c are also given. These loops exhibit similar magnetization (emu/cm^2) and coercive fields independent of the deposition potentials. Since the Ni substrate is ferromagnetic, the magnetization of the deposited layer will result in a very small effect on the weak coercive field.

Fig. 12 also shows the hysteresis loops of the electrodeposited layers on the Cu sheet, which were analyzed by VSM. Fig. 12 reveals that the coercive field H_c is 236.5 Oe when the deposition potential is -0.8 V, and that a higher Co content leads to a larger magnetization. However, it is conjectured that no reduction of Dy^{3+} to Dy has occurred judging from the low coercivity. Thus, how to improve the coercive field H_c still remains for further investigation. Besides, the temperature-dependent susceptibility will be investigated after the coercivity is promoted.

Conclusions

The sequence of conductivities for the different melts is $ZnCl_2$-EMIC > $ZnCl_2$-EMIC-$CoCl_2$ > $ZnCl_2$-EMIC-$DyCl_3$ > $ZnCl_2$-EMIC- $CoCl_2$-$DyCl_3$. The results may be explained in terms of the viscosity increase due to complex formation as cobalt chloride or dysprosium chloride are added into the acidic $ZnCl_2$-EMIC melt.

Cyclic voltammetry for the 50-50 mole% $ZnCl_2$-EMIC melt containing 1.687 mol% $CoCl_2$ and 1.114 mol% $DyCl_3$ on a Ni electrode at 100 °C and a Cu electrode at 80 °C has been carried out under different scan reverses. The morphology and composition of the electrodeposited layer have been analyzed by SEM and EDS, respectively. As the less negative deposition potential is applied, finer grains with a higher Co content were obtained. EDS results reveal that the electrodeposition of zinc is the major electrochemical reaction at more negative deposition potential. Hysteresis loops of electrodeposited layers were obtained by VSM analysis, which indicate that a higher Co content leads to a larger the magnetization. The larger coercivity is necessary for the preparation of MO thin film. How to improve the coercivity requires further studies.

[1] R. S. Beach, J. A. Borchers, A. Matheny, R. W. Erwin, M. B. Salamon, B. Everitt, K. Petit, J. J. Rhyne, C. P. Flynn, Phys. Rev. Lett. **70**, 3502 (1993).
[2] M. Sagawa, S. Fulimura, H. Y. Amamoto, Y. Matsuura, S. Hirosawa, J. Appl. Phys. **57**, 4094 (1985).
[3] Ch. V. Mohan, H. Kronmüller, J. Alloys Comp. **267**, L9 (1998).
[4] P. Papakonstantinou, B. Teggart, R. Atkinson, J. Mann. Magn. Mat. **163**, 378 (1996).
[5] Z.-Q. Lu, Z.-Y. Lee, Y.-K. Zheng, Z.-Q. Hu, G. Lin, Mater. Sci. Eng. B **76**, 50 (2000).
[6] R. A. Batey, D. A. Powell, A. Acton, A. J. Lough, Tetrahedron Lett. **42**, 7935 (2001).
[7] J. C. A. Huang, J. Cryst. Growth **1393**, 63 (1994).

[8] W. Kockelmann, W. Schager, J. K. Yakinthos, P. A. Kotsanidis, J. Magn. Magn. Mater. **177 – 181**, 792 (1998). C. Schubler-Langeheine, E. Weschke, H. Ott, A. Yu. Grigoriev, A. Moller, R. Meier, C. Mazumdar, G. Kaindl, J. Electron Spectros. Rela. Phenom. **114 – 116**, 795 (2001).
[9] Po-Yu Chen, I-Wen Sun, Electrochim. Acta **46**, 1169 (2001).
[10] H.-Y. Hsu, C.-C. Yang, Z. Naturforsch. **56a**, 670 (2001).
[11] T. Uda, T. H. Okabe, Y. Waseda, K. T. Jacob, J. Alloys Comp. **284**, 282 (1999).
[12] N. I. Usenko, M. I. Ivanov, J. Alloys Comp. **261**, L4 (1997).
[13] S. G. Sankar, V. U. S. Rao, E. Segal, W. E. Wallace, W. G. D. Frederick, H. J. Garret, Phys. Rev. **11**, 435 (1975).
[14] B. Scharitfker, G. Hills, Electrochim. Acta **28**, 879 (1983).
[15] A. J. Bard, L. R. Faulkner, Electrochemical Methods, Fundamentals and Applications, John Wiley & Sons, New York (1980).